Challenge Journal of
CONCRETE RESEARCH LETTERS

Vol.13 No.2 (2022)

acoustic emission aerated concrete compressive strength concrete corrosion cracking curing ductility durability energy absorption ferrocement fly ash fracture mechanical properties mortar nanoparticle palm oil fuel ash reinforced concrete self-compacting concrete silica fume strengthening superplasticizer tensile strength workability waste disposal water absorption

ISSN 2548-0928

TULPAR ACADEMIC PUBLISHING

Challenge Journal of Concrete Research Letters

E-mail: *cjcrl@challengejournal.com*

Web page: *cjcrl.challengejournal.com*

TULPAR Academic Publishing
www.tulparpublishing.com

Challenge Journal of Concrete Research Letters

CONTENTS

Research Articles

TULPAR ACADEMIC PUBLISHING

Challenge Journal of Concrete Research Letters

Research Article

Effect of curing time on polymer concrete strength

Ferit Cakir [a,*]

[a] *Department of Civil Engineering, Gebze Technical University, Gebze, 41400 Kocaeli, Turkey*

ABSTRACT

With the advancement of polymer technology, polymer concrete (PC) has become increasingly popular throughout the world and it has among the major construction materials due to its many advantages. The strength and durability of PCs are directly related to paste quality and curing time. The curing time is of the utmost importance to ensure desirable mechanical properties. An understanding of the strength-time relationship of PCs is crucial to understanding the effects of loading on concrete at an older age. The objective of this paper is to study the behavior of PC under different curing times with an emphasis on compressive and flexural strengths. Therefore, a total of 63 specimens were tested at seven different ages (1 day, 3 days, 5 days, 7 days, 14 days, 28 days, and 105 days) throughout the study. According to the results obtained from the tests, it is shown that the curing time plays a critical role in the flexural and compressive strengths of PCs. PCs gain more than 80% of their mechanical strength within three days, and the long-term strength does not change significantly after seven days.

ARTICLE INFO

Article history:
Received 28 January 2022
Revised 13 March 2022
Accepted 24 March 2022

Keywords:
Polymer concrete
Curing time
Compressive strength
Flexural strength

1. Introduction

Cement-based concretes (CBCs) are one of the most popular construction materials all around the world. Although these materials have many important characteristics such as high compressive strength and low cost, they have several limitations including low tensile strength, poor durability, and low chemical resistance. Hence, the search for new materials to replace CBCs and prepare concrete without cement are the most important research topic for civil engineering committees. CBC has been replaced by polymer-based concrete as the most popular alternative in the construction industry (Shaw 1985). In accordance with the American Concrete Institute (ACI), there are three types of polymer-based concretes; Polymer Portland Cement Concrete (PPCC), Polymer Impregnated Concrete (PIC), and Polymer Concrete (PC) (ACI 548.1R 2009). PPCC is a concrete mix that contains cement and polymer as binders. PPCCs are usually made by mixing polymer into fresh cement concrete (Justnes 2004; Czarnecki 2018). In PIC, hardened concrete is impregnated with polymers for 4–5 hours, and a polymer layer is formed around it (Kumar and Narayanan 2020). PC differs from PPCCs and PICs, as it lacks a cement binder and uses polymers instead of cement as a binder. Today, PCs have become the most emphasized materials since they do not contain cement. The most important characteristics of these materials are high pressure, tensile and shear strengths, as well as rapid hardening and surface hardness. Therefore, they can be effectively used in new and existing structures due to these superior properties (Bedi et al. 2013).

The quality of the mixture and the curing time determine the strength and durability of PCs. The curing period is one of the most important factors in determining the mechanical properties of the final product (Ohama and Demura 1982). The curing process has been proven by previous studies to be one of the most important steps to ensuring durable concrete. Particularly, early curing of concrete improves its performance considerably, so it is crucial to cure it appropriately of the start. Ohama and Demura (1982) emphasized that the compressive strength of polyester resin concrete generally increases with the addition of heat curing time, and virtually remains constant from about five to ten hours regardless of the amount of pre-curing time. Tae and Choi

* *Corresponding author*. Tel.: +90-262-605-1000 ; Fax: +90-262-653-8490 ; E-mail address: cakirf@gtu.edu.tr (F. Cakir)
ISSN: 2548-0928 / DOI: https://doi.org/10.20528/cjcrl.2022.02.001

(2012) focused on the time-dependent behavior of polymer concrete using unsaturated polyester resin. It was concluded from the study that recycled unsaturated polyester resin-based polymer concrete achieved over 80% of its 28-day strength in seven days. Hoe Kwen et al. (2015) conducted an experimental study on accelerated curing regimes for polymer-modified cement. In the study, it was found that samples exposed to 8 hours of hygrothermal treatment were comparable to those exposed to 24 hours of treatment. Khalid et al. (2015) studied the effect of curing temperature and period on apparent density, compressive strength, and morphology properties of PCs. According to the study, PC based on the orthophthalic and isophthalic polymers had higher compressive strength when cured for at least six hours and three hours, respectively at cure temperatures of 50 °C and 70 °C. The compressive strength reached its maximum at 30 °C only after 16 hours of curing. Hong (2017) investigated the effects of curing temperature and curing time on the mechanical properties of polysulfide PC. According to this study, approximately 27% of the compressive strength of curing polysulfide PC formed within 6 hours and approximately 80% within 7 days of curing.

2. Materials and Method

A series of experiments was conducted to investigate the effects of curing time on the mechanical properties of the hardened PCs. In all mixes, all constituents were kept in a constant proportion by weight. This study utilized natural fine aggregate, polyester resin, acetylacetone peroxide (AAP) and cobalt naphthenate to prepare a composite material.

2.1. Aggregate

Natural fine aggregates of three different sizes, obtained from Istanbul and Kirklareli, Turkey, were used in the study. In order to eliminate contamination, all aggregates were cleaned thoroughly with clear water and naturally dried before use. The chemical composition of the aggregates is listed in Table 1.

2.2. Binder

In the scope of the study, general-purpose unsaturated polyester resin (UPR) with high filling wetting power was used. UPRs are thermosetting and can be cured from a liquid to a solid with the right conditions. Polyester resins account for the majority of resins used in the world today. The main polymeric chain of this resin contains ester bonds, which are formed by the compaction of a multifactorial alcohol compound and its multifactorial acid. The technical properties of the UPR are given in Table 2.

2.3. Hardener

During this study, acetylacetone peroxide, a fast-curing peroxide commonly used to cure unsaturated polyester resins, was used. Table 3 presents the technical information about the hardener.

Table 1. Chemical composition of the natural fine aggregates.

Chemicals	Aggregates		
	0.3-1 mm	1-3 mm	3-5 mm
MgO	0.10	0.06	0.06
Al_2O_3	0.245	1.80	1.86
SiO_2	98.86	94.20	94.15
CaO	0.01	0.45	0.39
Fe_2O_3	0.148	0.46	0.46
SO_3	-	0.10	0.10
K_2O	0.03	1.52	1.56
Na_2O	0.02	1.16	1.12
Ignition Loss	0.24	0.25	0.30

Table 2. Technical properties of the UPR.

Properties	Values
Flexural strength in 5% strain (MPa)	51.6
Compressive strength (MPa)	34.1
Impact strength (J/m)	12.9
Viscosity (mPa.s)	659
Shore hardness	80
Tensile modulus (MPa)	527
Density (g/cm^3)	1.225

Table 3. Technical properties of the hardener.

Properties	Values
Flash point	>60°C
Density, 20°C	1055 kg/m^3
Viscosity, 20°C	21 mPa.s
Self-accelerating decomposition temperature (SADT)	60 °C
Total active oxygen	4.0-4.2%
Peroxide content	33%
Diethylene glycol + water + diacetone alcohol	67%

2.4. Accelerator

Accelerators are used to speed up the reaction between the resin and the hardener. In general, accelerators raise the temperature in a system, which speeds up epoxy reactions. An accelerator for activating the curing agent was selected in this study as cobalt naphthenate. Table 4 presents technical information about the accelerator.

Table 4. Technical properties of the accelerator.

Properties	Values
Density	0.92 g/cm^3 (20°C)
Viscosity	300 mPa.s (20°C)
Self-accelerating decomposition temperature (SADT)	≥150°C
Flash point	62°C
Cobalt content	1.5%

3. Experimental Studies

Compression, flexural and density tests were performed to evaluate the hardened concrete properties. All tests were performed according to the ASTM specifications. A total of 42 concrete samples, consisting of 21 samples for flexural and 21 samples for compression tests, was cast and tested on the 1 day, 3 days, 5 days, 7 days, 14 days, 28 days, and 105 days of curing age for compressive strength and flexural strength. In the compressive and flexural strength tests, the hardened samples were tested until failure by using the Form-Test machine with 600 kN (Fig. 1). The experimental program in this study was conducted in the Research and Development (R&D) Engineering Laboratory at Mert Casting Inc., Turkey. The data obtained from the hardened concrete tests are summarized in Tables 5-11.

Fig. 1. Experimental studies.

Table 5. Mechanical properties at the curing age of 1 day.

Sample	Curing Time	Sample Weight	Sample Dimensions (mm)			Maximum Flexural Load	Flexural Strength	Maximum Compressive Load	Compressive Strength
	Days	(gr)	X	Y	Z	(kN)	(MPa)	(kN)	(MPa)
1	1	568.11	40	40	155	5.06	11.86	71.12	44.45
2	1	567.04	40	40	155	4.97	11.65	70.81	44.26
3	1	568.99	40	40	155	4.89	11.46	77.72	48.58
					Average	4.97	11.66	73.22	45.76

Table 6. Mechanical properties at the curing age of 3 days.

Sample	Curing Time	Sample Weight	Sample Dimensions (mm)			Maximum Flexural Load	Flexural Strength	Maximum Compressive Load	Compressive Strength
	Days	(gr)	X	Y	Z	(kN)	(MPa)	(kN)	(MPa)
1	3	566.16	40	40	155	8.88	20.81	136.12	85.08
2	3	569.54	40	40	155	8.87	20.79	139.81	87.38
3	3	566.95	40	40	155	8.87	20.79	136.72	85.45
					Average	8.87	20.80	137.55	85.97

Table 7. Mechanical properties at the curing age of 5 days.

Sample	Curing Time	Sample Weight	Sample Dimensions (mm)			Maximum Flexural Load	Flexural Strength	Maximum Compressive Load	Compressive Strength
	Days	(gr)	X	Y	Z	(kN)	(MPa)	(kN)	(MPa)
1	5	567.68	40	40	155	10.33	24.21	147.82	92.39
2	5	566.17	40	40	155	9.97	23.37	149.15	93.22
3	5	564.6	40	40	155	10.17	23.84	148.88	93.05
					Average	10.16	23.80	148.62	92.89

Table 8. Mechanical properties at the curing age of 7 days.

Sample	Curing Time	Sample Weight	Sample Dimensions (mm)			Maximum Flexural Load	Flexural Strength	Maximum Compressive Load	Compressive Strength
	Days	(gr)	X	Y	Z	(kN)	(MPa)	(kN)	(MPa)
1	7	567.67	40	40	155	13.36	31.31	157.73	98.58
2	7	568.40	40	40	155	12.96	30.38	156.94	98.09
3	7	563.99	40	40	155	12.03	28.20	161.22	100.76
					Average	12.78	29.96	158.63	99.14

Table 9. Mechanical properties at the curing age of 14 days.

Sample	Curing Time	Sample Weight	Sample Dimensions (mm)			Maximum Flexural Load	Flexural Strength	Maximum Compressive Load	Compressive Strength
	Days	(gr)	X	Y	Z	(kN)	(MPa)	(kN)	(MPa)
1	14	571.67	40	40	155	14.31	33.54	163.03	101.89
2	14	568.74	40	40	155	13.98	32.77	164	102.50
3	14	559.89	40	40	155	14.05	32.93	163.26	102.04
					Average	14.11	33.08	163.43	102.14

Table 10. Mechanical properties at the curing age of 28 days.

Sample	Curing Time	Sample Weight	Sample Dimensions (mm)			Maximum Flexural Load	Flexural Strength	Maximum Compressive Load	Compressive Strength
	Days	(gr)	X	Y	Z	(kN)	(MPa)	(kN)	(MPa)
1	28	561.61	40	40	155	14.55	34.10	163.88	102.43
2	28	570.74	40	40	155	14.50	33.98	164.89	103.06
3	28	569.96	40	40	155	14.21	33.30	163.67	102.29
					Average	14.42	33.80	164.15	102.59

Table 11. Mechanical properties at the curing age of 105 days.

Sample	Curing Time	Sample Weight	Sample Dimensions (mm)			Maximum Flexural Load	Flexural Strength	Maximum Compressive Load	Compressive Strength
	Days	(gr)	X	Y	Z	(kN)	(MPa)	(kN)	(MPa)
1	105	567.50	40	40	155	14.65	34.34	165.61	103.51
2	105	568.98	40	40	155	14.51	34.01	166.25	103.91
3	105	569.01	40	40	155	14.74	33.38	167.77	104.86
					Average	14.63	33.91	166.54	104.09

When focusing on the mechanical tests performed on the hardened concrete tests, it was seen that the compressive strength of the samples varies between approximately 45.76 MPa and 104.09 MPa at 1 day and 105 days, respectively (Fig. 2). According to the average compressive strengths, the PCs gain more than 40% of their strength 1 day after pouring. Within 3 days, PCs gained more than 80% of their compressive strength, and long-term compressive strength did not significantly change after 7 days (Fig. 2). When the flexural strengths of the samples were examined, the average flexural strength obtained on the 1st day was 11.66 MPa, while the average flexural strength obtained on the 105th day was 34.30 MPa (Fig. 3). When the time-dependent variation was examined, the long-term flexural strength of the materials became significantly unchanged after 7 days, as did the compressive strength of the materials (Fig. 4). When focusing on the densities of the materials, it was determined that the densities of the materials were generally very close to each other and the density to the medium was 568 gr/cm^3. In addition, it was seen that there was no significant time-dependent change in densities in general (Fig. 5). The results obtained in this study were examined to the results of studies carried out in the literature. Based on the examination, Tae and Choi (2012) concluded that the unsaturated polyester resin-based polymer concrete achieved over 80% of its 28-day strength in 7 days. Similarly, Hong (2017) emphasised the approximately 27% of the compressive strength of curing polysulfide PC formed within 6 hours and approximately 80% within 7 days of curing.

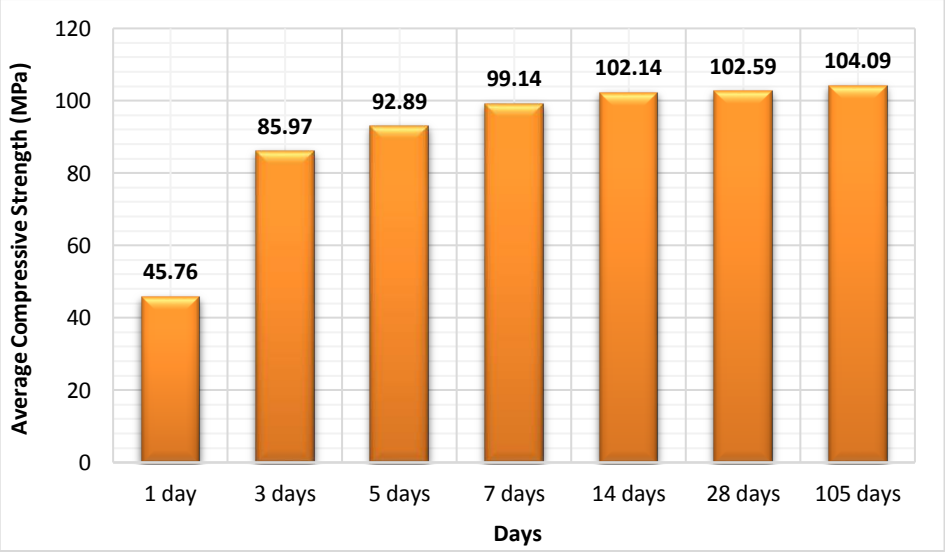

Fig. 2. The average compressive strengths (MPa).

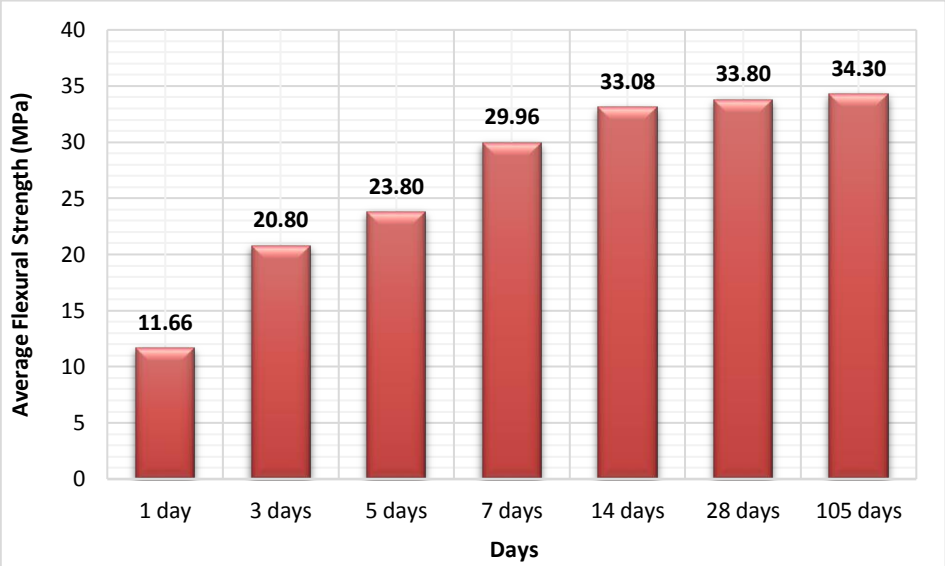

Fig. 3. The average flexural strengths (MPa).

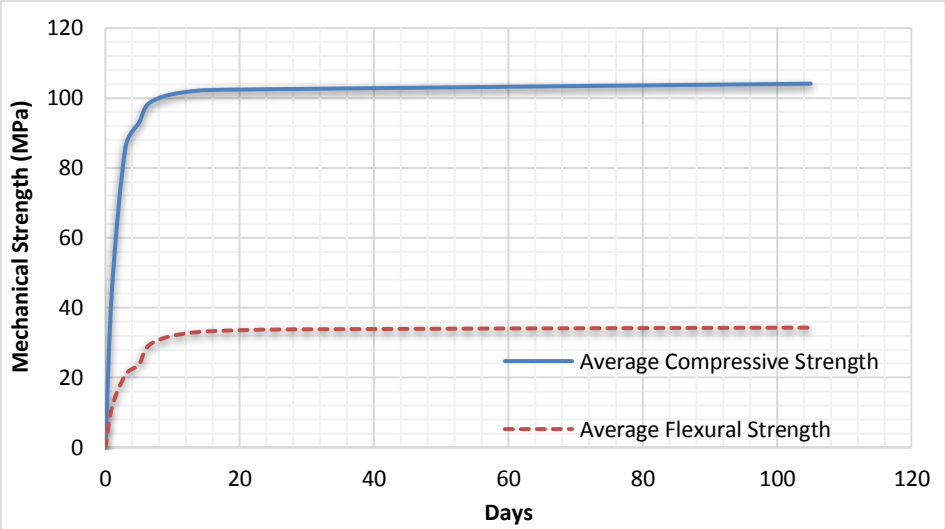

Fig. 4. Comparison between the average compressive and flexural strength considering the curing time.

Fig. 5. The average densities (gr/cm^3).

Comparing the results obtained from PCs with those obtained from cement-based concrete (CBC), it turns out that PCs gain strength earlier than CBCs. The American Concrete Institute (ACI) Committee emphasizes that the majority of the mechanical strength of cement-based concretes reached in 28 days (ACI 308R-01 2008). Figs. 6a and 6b illustrate the relationship between compressive strength and curing temperature, and the relationship between long-term compressive strength and curing age of CBCs.

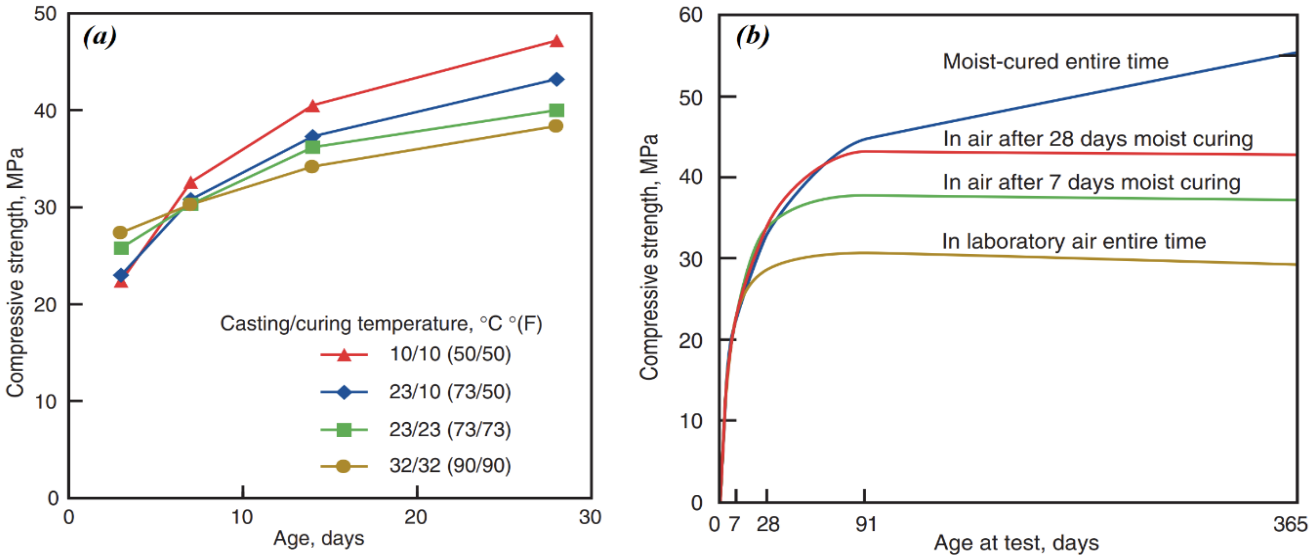

Fig. 6. a) Relationship between a compressive strength curing temperature;
b) Relationship between a long-term compressive strength and curing age of CBCs (Kosmakta et al. 2008).

4. Conclusions

Polymer concretes (PCs) have become increasingly common in many different industries in recent years and they are generally used as special concrete in various construction applications. PCs are seen as the best alternative to cement concrete because of their high performance. Compared to the CBCs, PCs produce a very different type of product. While cement is used as a binder material in CBCs, resins are used as binders in PCs. This study mainly focuses on the effect of curing age on PC strength and the paper explains how different curing times affect PC strength.

After performing mechanical tests on the hardened concrete samples, a compressive strength ranging from approximately 45.76 MPa to 104.09 MPa was determined at one day and 105 days, respectively. Based on the average compressive strength, PCs gain more than 40% of their strength a day after pouring. After three days, PCs regained more than 80% of their compressive strength, and their long-term strength remained unchanged after seven days. The flexural strength of 11.66 MPa was recorded on the 1st day, while the strength of 34.30 MPa was measured on the 105th day. After 7 days, the flexural and compressive strengths of the materials were unchanged considering the time-dependent variation. Regarding the densities, it was found that the materials have generally very close densities and that the density of the average is 568 g/cm^3. In general, it was found that densities did not change significantly with time.

Acknowledgements

The author would like to thank Mert Casting Inc. for its continuous support during the study.

Funding

The author received no financial support for the research, authorship, and/or publication of this manuscript.

Conflict of Interest

The author declared no potential conflicts of interest with respect to the research, authorship, and/or publication of this manuscript.

References

ACI 308R-01 (2008). Guide to Curing Concrete. American Concrete Institute, Farmington Hills, MI, USA.

ACI 548.1R (2009). Guide for the use of polymers in concrete. American Concrete Institute, Farmington Hills, MI, USA.

Bedi R, Chandra R, Singh SP (2013). Mechanical properties of polymer concrete. *Journal of Composites,* 2013, 1–12.

Czarnecki L (2018). Polymer-Concrete composites for the repair of concrete structures. *Proceedings of the MATEC Web of Conferences, EDP Sciences - Web of Conferences*, France.

Hoe Kwan W, Ramli M, Ban Cheah C (2015). Accelerated curing regimes for polymer-modified cement. *Magazine of Concrete Research,* 67, 1233–1241.

Hong S (2017). Influence of curing conditions on the strength properties of polysulfide polymer concrete. *Applied Sciences*, 7(8), 833.

Justnes H (2004). Polymer cement concrete (PCC) of interest for concrete block paving? http://sept.org/techpapers/521.pdf

Khalid NHA, Hussin MW, Ismail M, Ismail MA, Mohamed A, Ariffin NF, Lim NHAS, Samadi M (2015). Effect of post-curing regime on density, compressive strength and crosslinking of polymer concrete. *Jurnal Teknologi,* 77(12), 31–35.

Kosmakta SH, Kerkhoff B, Panarese WC (2018). Design and Control of Concrete Mixtures. Fourteenth Edition, Engineering Bulletin, Portland Cement Association, Chicago, USA.

Kumar GR, Narayanan VR (2020). A review on polymer impregnated concrete using steel wire mesh. *Materials Today: Proceedings*, 33, 338–344.

Ohama Y, Demura K (1982). Relation between curing conditions and compressive strength of polyester resin concrete. *International Journal of Cement Composites and Lightweight Concrete,* 4, 241–244.

Shaw JDN (1985). Resins in construction. *International Journal of Cement Composites and Lightweight Concrete,* 7, 217–223.

Tae GH, Choi ES (2012). Time dependent behavior of polymer concrete using unsaturated polyester resin. From The Edited Volume, *Polyester, Edited by Hosam El-Din M. Saleh*, IntechOpen.

Challenge Journal of Concrete Research Letters

Research Article

Research on micro limestone for concrete pavements produced with natural aggregates in the Erzurum region

Ali Öz [a,*]

[a] *Department of Construction, Narman Vocational School, Atatürk University, 25530 Erzurum, Turkey*

ABSTRACT

The use of naturally formed aggregates in concrete pavements is an innovative and sustainable solution both environmentally and economically. This study investigates the usability of fine and coarse aggregates formed spontaneously in Oltu, Narman, Pasinler and Uzundere in concrete pavements by improving the mechanical properties of concrete. In the study, the compressive strength, flexural strength, water absorption capacity and capillarity permeability of the concrete samples planned to be used on concrete pavements were obtained by considering the contribution of these aggregates. In addition, microscopic electron scanning analyzes (SEM) were applied to visualize the internal cracks that may occur in the concrete. The test results showed that the concrete formed with aggregates from Oltu and Pasinler regions had the highest compressive, flexural and hardened unit weights. It has been concluded that the concrete produced from Uzundere region, which gives results below 35 MPa in terms of compressive strength, is not applicable on concrete pavements. In addition, considering the high compressive, flexural, unit weight and capillary permeability, it is predicted that the most suitable concrete design for the construction of concrete pavements is the P_0 (concrete formed with aggregates from Pasinler region) concrete sample.

ARTICLE INFO

Article history:
Received 19 April 2022
Revised 25 May 2022
Accepted 2 June 2022

Keywords:
Concrete pavements
Natural aggregates
Mechanical properties
Microstructural analysis

1. Introduction

Today, concrete pavements, formed with cement as a binding material, are a type of coating used on pavements exposed to medium and heavy traffic loads. Concrete pavements are examined in joint-free concrete pavement, joint-reinforced concrete pavement, and joint-free reinforced concrete pavement. In addition, concrete pavements can be formed as pre-stressed concrete, compacted with rollers and composite (Budak et al. 2009). Concrete pavements have advantages such as long structural life, being economical, being stiffness and having high strength, being applicable in all conditions, providing fuel savings and being costly (Kozak 2011). With innovations and rapid developments in concrete pavement technology such as ready-mixed concrete, slip form, permeable concrete, fiber concrete, pre-stressed concrete, and continuously reinforced concrete, concrete pavements have become an indispensable option against asphalt pavements for today's modern roads (Şengün et al. 2020). Generally, as an alternative to asphalt pavements, roller compacted concrete pavement is preferred because of its stiffness and non-collapsing, fast construction and efficiency (Nanni et al. 1996). Concrete, which forms the formation of roller-compacted concrete pavements, has a high volume of fine aggregate, low volume of binder, coarse aggregate and water (Lam et al. 2018).

Population growth, rapid urbanization and continuous economic developments create some basic needs in transportation (Strieder et al. 2022). To meet these needs, it is necessary to put forward innovative approaches in the transportation sector by using naturally occurring components. Bitumen, a product of petroleum decomposition, is used in the transportation field to reduce the decomposition of aggregates by interlocking

* *Corresponding author*. Tel.: +90-442-741-5233 ; Fax: +90-442-741-3334 ; E-mail address: alioz@atauni.edu.tr (A. Öz)
ISSN: 2548-0928 / DOI: https://doi.org/10.20528/cjcrl.2022.02.002

and to reduce the water permeability of asphalt coatings (Airey 2002). However, bitumen that undergoes age-hardening has lower penetration and higher viscosity. As a result, bituminous pavement layers may deteriorate because the bituminous binder hardens and becomes more brittle and its adhesion with the aggregate decreases (Isacsson and Lu 1995; Suo and Wong 2009). In addition, considering that bitumen is a more costly material, concrete coatings have been considered a new alternative to asphalt coatings in recent years (Harrington et al. 2010; Komastka et al. 2003). In the concrete design to be used in the construction of concrete pavements developed as an alternative to asphalt pavements, the relevant standards (ASTM C944 2019) should be considered and with environmental conditions and application (Ebrahimi Besheli et al. 2021). In addition, attention should be paid to the compressive strength, durability, and tensile strength in flexural and non-wearing concrete, which is the main component of concrete pavements (Ebrahimi Besheli et al. 2021). In this context, to provide optimum mechanical properties in concrete, the design of binders, aggregates, plasticizers and set accelerator additives and solutions constituting concrete formation should be made. It is also recommended that the compressive strength of the concrete to be used in the construction of concrete pavements be higher than 35 MPa and the flexural strength higher than 5 MPa (Lee et al. 2005).

Researchers have conducted different studies on concrete pavements and concrete, one of the basic components that make up concrete pavements. Studies have shown that concrete pavements designed with aggregates obtained by recycling from construction and demolition wastes provide low energy consumption, less cost and optimum mechanical properties (Delongui et al. 2018; Lee et al. 2005; Sangiorgi et al. 2015). Reducing permeable surfaces in concrete pavements causes an imbalance in the hydrological cycle, reducing water seepage and significantly increasing runoff, which causes flooding due to excessive loads in the storm-water drainage system. To cope with these adverse situations, a permeable concrete consisting of rationally graded coarse aggregates with a minimum amount of aggregate and sufficient cement content to provide an optimum coating around aggregates without additives has been designed (American Concrete Institute 2010; Chandrappa and Biligiri 2016). Strieder et al. (2022) evaluated the performance of porous concrete pavements with recycled concrete aggregate. The study analyzed concrete permeability, hardened density, hydraulic conductivity, seepage, compressive and tensile strengths, abrasion resistance, modulus of elasticity, and Poisson's ratio. Laboratory study results showed that the replacement of recycled concrete aggregates (RCA) improves hydraulic properties and reduces mechanical behavior (Strieder et al. 2022). Keles et al. (2022) investigated the strength properties of roller compacted concrete pavement (RCCP) under different curing methods. According to the results obtained, it was determined that the best curing method for the compressive and flexural strengths of RCCP is water curing, which provides approximately 29% and 34% increase in strength compared to uncured mixtures (Keleş and Akpinar 2022). Eisa et al. (2022) investigated the use of metakaolin-based geopolymer concrete in concrete pavements. To determine how geopolymerization contributes to the mechanical properties of concrete used in concrete pavements, such as compression, flexural and tensile in bending, the mechanical properties of concrete produced with conventional Portland cement and the mechanical properties of metakaolin-based geopolymer concrete were compared. It was observed that geopolymer concrete pavements reached compressive strengths of 30.3 MPa and 32.3 MPa on the 7th and 28th days, respectively. In contrast, the conventional Portland cement concrete pavements reached a compressive strength of 14.0 and 33.1 MPa on the 7th and 28th days, respectively. The results showed that metakaolin-based geopolymer concretes are more suitable for use in concrete pavements than Portland cement concrete to achieve higher strength values, be less energy consumption, and be more environmentally friendly (Eisa et al. 2022). Acar (2022) investigated the usability of naturally formed Kayseri volcanic slags as filling material in flexible paved roads. The results showed that the geotechnical properties of volcanic slags could be improved by stabilizing them with cement, and it can be used as a construction material in the base fill, sub-base and foundation layers of flexible paved roads and all kinds of fillings (Acar 2022). Yıldız (2012) investigated the usability of self-forming pumice and zeolite added to concrete in road pavements. Wet concrete tests, hardened concrete tests and abrasion tests were carried out on high-strength concretes containing pumice and zeolite with different mixing ratios. The results showed that all mixtures met the minimum concrete strength values and wear limit values specified in ASTM C944 (2019).

In this study, the usability of natural aggregates in the Erzurum region on concrete pavements was investigated. Because concrete pavements that can be produced with local resources will be more economical. Therefore, the physical, mechanical and microstructural properties of concretes that can be used in concrete pavements production were investigated.

2. Experimental Studies

2.1. Material

The type of cement used in the study is CEM I 42.5 R according to the TS EN 197-1 Standard (EN197-1 2004). Micro limestone was used in the mixtures to reduce cement's environmental impact and increase its water absorption capacity (Bekem Kara 2020). The physical and chemical properties of cement and micro limestone are given in Table 1.

The mixture's aggregate is presented in Fig. 1 as 0-5 mm river sand, 0-5 mm stone dust, 5-15 mm fine gravel, 15-25 mm coarse aggregate. Each aggregate conforming to the ASTM C33 (ASTM C33 2016) standard was obtained from the Narman, Oltu, Pasinler and Uzundere regions. The sieve analysis of the blended aggregates used in concrete mixes is presented in Fig. 1. The mixing ratios of the blended aggregates in Fig. 1 are given in Table 2.

Particle sizes, specific gravity, water absorption capacities and fineness modules of naturally supplied aggregates are given in Table 2. Aggregates used in concrete mixtures are given in Fig. 2. In addition, water-reducing/plasticizer CHRYSO®Delta SL-T chemical additive was used to ensure that the hydration reactions in the mixtures were homogeneously at every point of the concrete and improved the strength and durability.

Table 1. Physical and chemical properties of cement and micro limestone used in the study.

Material		CEM I 42.5 R	Micro Limestone
Physical and Mechanical Properties			
Blaine's Fineness (cm^2/g)		3532	4780
Specific Gravity (gr/cm^3)		3.12	2.70
Setting (min)	Initial	155	-
	Finally	215	-
Compressive Strength (MPa)	7 days	26.7	-
	28 days	55.1	-
Chemical Components (%)			
SiO_2		18.99	1.67
Al_2O_3		4.62	0.40
Fe_2O_3		3.36	0.36
CaO		63.4	53.01
MgO		1.83	-
SO_3		2.80	-
Na_2O		0.27	-
K_2O		0.86	-
Glow Loss		2.17	-
Free CaO		0.7	-

Table 2. Physical properties of aggregates from different regions used in the study.

Region	Aggregate Size (mm)	Capacity of Water Absorption (%)	Modulus of Fineness
Narman	0-5 mm river sand (%55)	2.61	2.56
	5-15 mm fine aggr. (%25)	2.58	5.02
	15-25 mm coarse aggr. (%30)	2.59	6.13
Oltu	0-5 mm river sand (%30)	2.62	2.68
	0-5 mm stone powder (%25)	2.60	2.89
	5-15 mm fine aggr. (%19)	2.61	5.25
	15-25 mm coarse aggr. (%26)	2.60	6.47
Pasinler	0-5 mm river sand (%30)	2.59	2.14
	0-5 mm stone powder (%23)	2.60	2.89
	5-15 mm fine aggr. (%20)	2.61	5.95
	15-25 mm coarse aggr. (%27)	2.59	6.90
Uzundere	0-5 mm river sand (%57)	2.55	2.30
	5-15 mm fine aggr. (%24)	2.56	5.04
	15-25 mm coarse aggr. (%29)	2.54	6.61

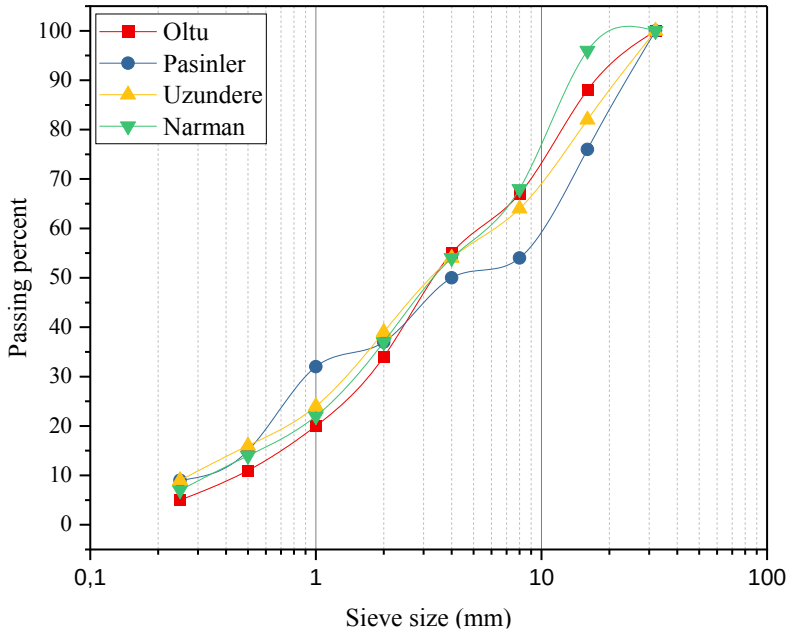

Fig. 1. Sieve analysis of the blended aggregates.

Fig. 2. Aggregates used in the concrete mix.

2.2. Mix design and curing

The mixture design of concretes formed with binder cement, micro limestone, chemical additives and related aggregates, the physical and chemical properties given in Tables 1 and Table 2, are made according to TS EN 12350-2 (2009) Standard and shown in Table 3.

Table 3 shows Narman mixture without N_0 micro limestone additive, Narman mixture with N_{10} limestone, Oltu mixture without O_0 limestone additive, Oltu mixture with O10 Pasinler mixture without P_0 limestone additive, Pasinler mixture with P_{10} limestone additive, Uzundere mixture without U_0 limestone additive. And U_{10} represents the Uzundere mix with limestone additives. The amount of material specified in Table 3 was placed in the manual cement mixer, and the mixture was created. First, cement, river sand, stone powder, aggregate and chemical additives were mixed in a cement mixer in a dry environment for 3 minutes. Then, water was added to the mixture, and the mixture was mixed for 3 minutes. The concrete extracted from the mixer was placed in 15x15x15 cm cube and 7x7x28 cm prism molds (beam mold). Beam and cube samples were kept in a water curing environment until the concrete gained strength on the 7th and 28th days. The samples removed from the water-cured environment were made ready for the hardened concrete tests. The production phase of concrete samples is shown in Fig. 3.

Table 3. Mixing ratios in 1 m^3 of concrete (kg/m^3).

Mixing	Cement	Water	Chemical Additive	Micro Limestone	0-5 River Sand	0-5 Stone Powder	5-15 Fine Aggregates	15-25 Coarse Aggregates
N_0	300	192	3	-	979	-	362	487
N_{10}	270	192	3	30	992	-	367	494
O_0	300	189	3	-	565	456	350	476
O_{10}	270	189	3	30	573	463	354	483
P_0	300	164	3	-	578	435	381	510
P_{10}	270	164	3	30	586	440	386	517
U_0	300	181	3	-	925	-	391	535
U_{10}	270	181	3	30	937	-	396	542

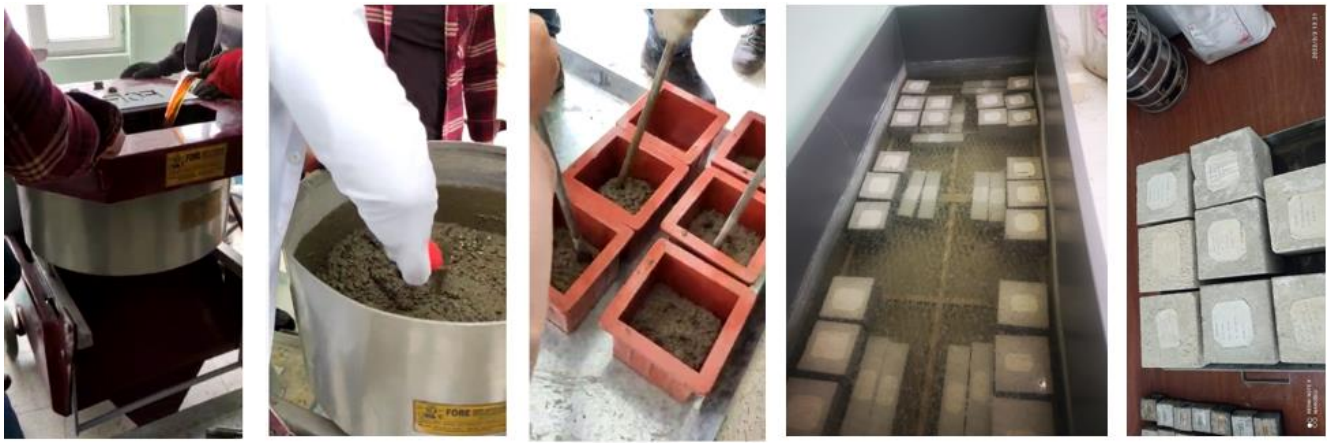

(a) (b) (c) (d) (e)

Fig. 3. Production stages of the concrete samples: a) Preparing the mixture in the mixer; b) Removing the mixture from the mixer; c) Molding the prepared mixture; d) Keeping the concrete samples in the curing environment; e) Concrete samples whose production has been completed.

2.3. Test procedures

According to TS EN 12390-2 (2009) Standard, the consistency determination for fresh concrete mixes was made. The hardened unit volume weights of the concrete samples formed with the aggregate samples taken from different regions were measured according to the ASTM C642 Standard (1997). The mechanical properties of compressive and flexural strength of 15x15x15 cm cube and 7x7x28 cm beam concrete samples were determined according to ASTM C348 (1998) and ASTM C349 (2002) Standards, respectively (Fig. 4). To examine the effects of concrete samples formed with different mixtures on the capillarity water absorption capacity of concrete pavements, the Capillarity water absorption capacities were calculated according to the EN 1015-18 Standard. Capillarity water absorption of fresh concrete mixes was measured in 15x15x15 cm cube samples in the first 24 hours (Fig. 5). Microscopic electron scanning (SEM) was performed to determine the microstructural properties of possible cracks in the concrete samples. Microstructure analyzes were taken at Kastamonu University MERLAB unit. SEM images of the mixtures at different magnifications were determined by Quanta device.

3. Discussion and Results

3.1. Physical properties

Fig. 6 shows that the hardened unit weights of concrete mixes on concrete pavements vary between 2257-2335 kg/m^3. It has been observed that the unit volume weights of the hardened concrete samples are very close to each other. It has been determined that micro limestone in mixtures reduces the hardened unit weight. It was determined that the unit weights of the concrete samples formed with the aggregates taken from the Narman region were 0.38%, 1.02% and 2.87% higher than the calculated unit weights of the concrete samples formed with the aggregates taken from the Oltu, Pasinler and Uzundere regions, respectively. It is understood that the reduction of the hardened unit weights of the concrete samples is negligible. Because the specific gravity of natural aggregates obtained from Erzurum region is close to each other. Therefore, no significant difference was observed between the hardened unit weights of the concrete mixtures.

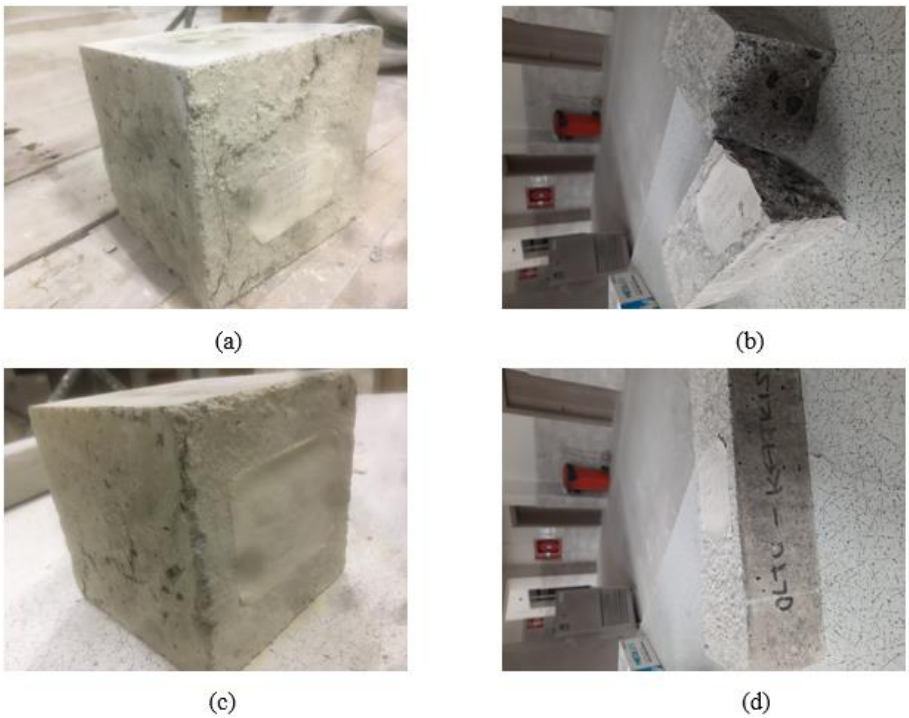

Fig. 4. Hardened concrete tests: a) Micro limestone cube sample; b) Micro limestone beam sample; c) Micro limestone-free cube sample; d) Micro limestone beam sample.

Fig. 5. Capillarity water absorption experiments.

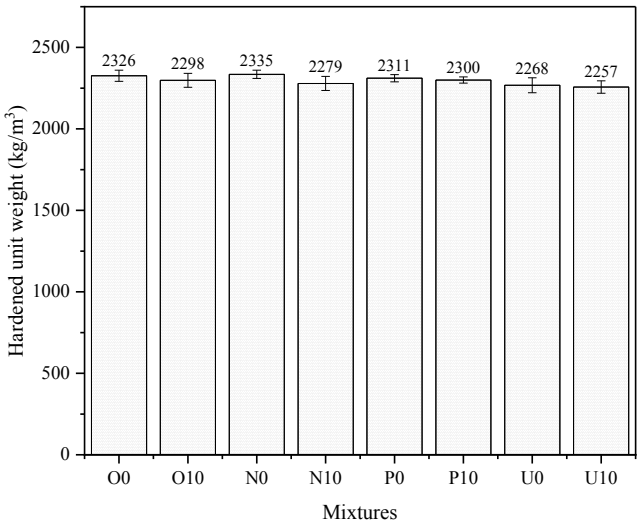

Fig. 6. Hardened unit weights of concrete samples.

3.2. Mechanical properties

According to the hardened concrete tests, Fig. 7 shows that the compressive strength of the concrete mixtures varies between 23.5-44.6 MPa, and the flexural strength varies between 2.93-4.27 MPa.

Generally, it has been determined that micro limestone in concrete mixtures reduces concrete's compressive and flexural strength. It has been observed that the highest compressive strength is in the concrete samples formed with fine and coarse aggregates taken from the Pasinler region without using micro limestone. It was observed that the 28-day concrete compressive strength of the concrete formed with the aggregates taken from Pasinler region was 44.6 MPa and the 7-day concrete compressive strength was 35.5 MPa. It was determined that the compressive strength of the concrete formed with the aggregates taken from Pasinler region was 0.22%, 9.64% and 26.45% higher than the compressive strength of the concrete formed with the aggregates taken from the Oltu, Narman and Uzundere regions, respectively. In terms of compressive strengths, it was observed that the most suitable mixture for concrete pavements, among the concrete mixtures designed in this study, was the concrete mixture formed with aggregates taken from Pasinler region, and concrete mixtures formed with aggregates taken from Uzundere region were not suitable. In addition, it was determined that the

strength of the concrete formed with aggregates from the Oltu region, with a flexural strength of 4.27 MPa, is higher than the strength of the concrete formed with aggregates from Pasinler, Narman and Uzundere. It has been determined that the flexural strength of the concrete formed with the aggregates taken from Oltu region is 5.62%, 9.13% and 6.86% higher than the compressive strength of the concrete formed with the aggregates taken from Pasinler, Narman and Uzundere regions, respectively. In addition, as the unit weights of the mixtures decrease, their compressive and flexural strengths decrease. The reduction in unit weight indicates that the porosity is relatively increased. Therefore, the mechanical properties of concretes are adversely affected. In Fig. 8, the flexural strength of concrete samples increases linearly with increased compressive strength. Generally, there is a direct proportionality between the compressive strength of concrete and other mechanical properties. Therefore, as the compressive strength increases, the flexural strength of concrete increases.

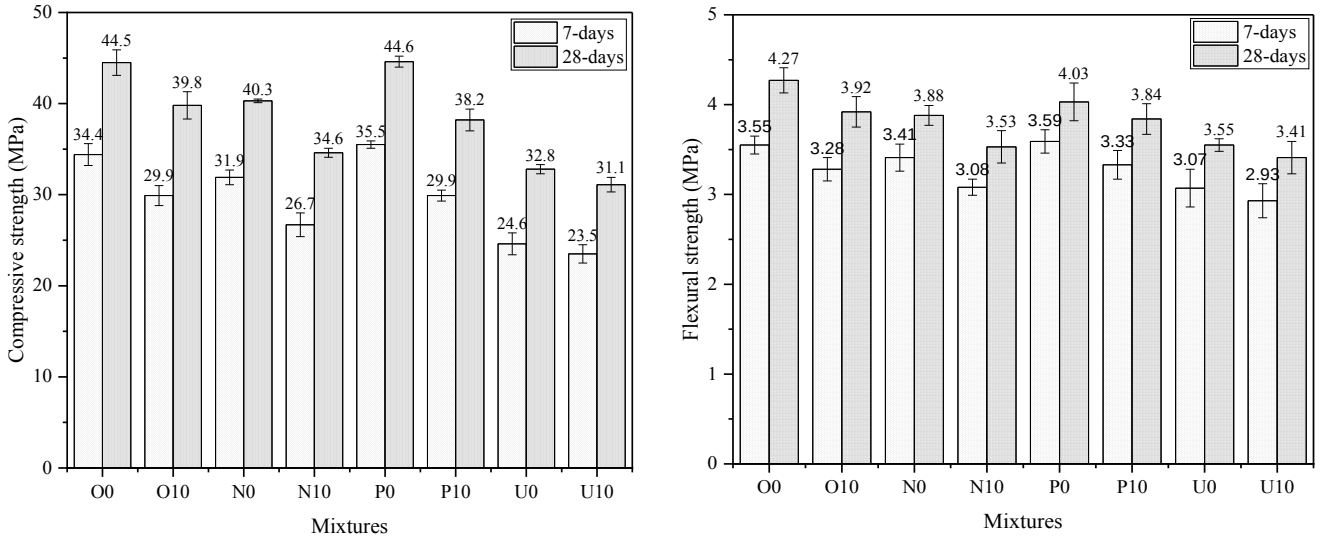

Fig. 7. Compression and flexural strength test results.

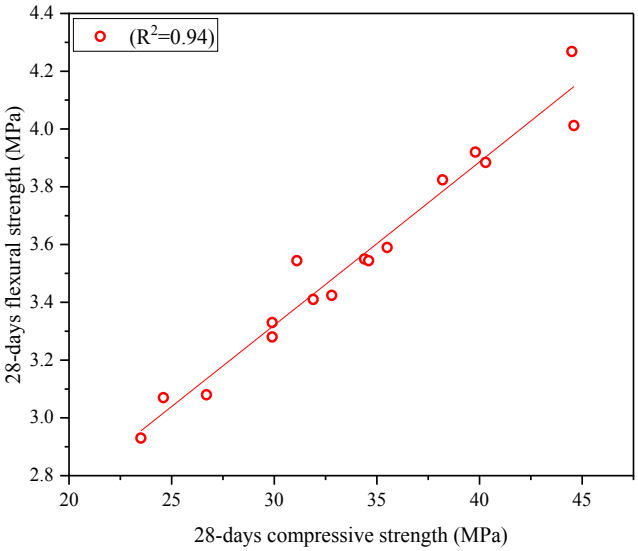

Fig. 8. Relationship between compressive and flexural strengths.

3.3. Capillarity water absorption capacities

Fig. 9 shows the capillarity water absorption capacities of concrete mixtures. It was observed that the capillarity water absorption capacities of the mixtures were below 1.26 kg/m². It was determined that the concrete mixture with the highest capillarity water absorption was U_{10} with a value of 1.26 kg/m² and the mixture with the lowest capillarity water absorption was O_0 with a value of 0.13 kg/m². It has been determined that the capillarity water absorption of the concrete formed with the aggregates taken from the Oltu region is 62.85%, 23.52% and 86.45% less than the capillarity water permeability of the concretes formed with the aggregates taken from the Narman, Pasinler and Uzundere regions, respectively. It has also been determined that micro limestone in mixtures increases the capillarity of water absorption.

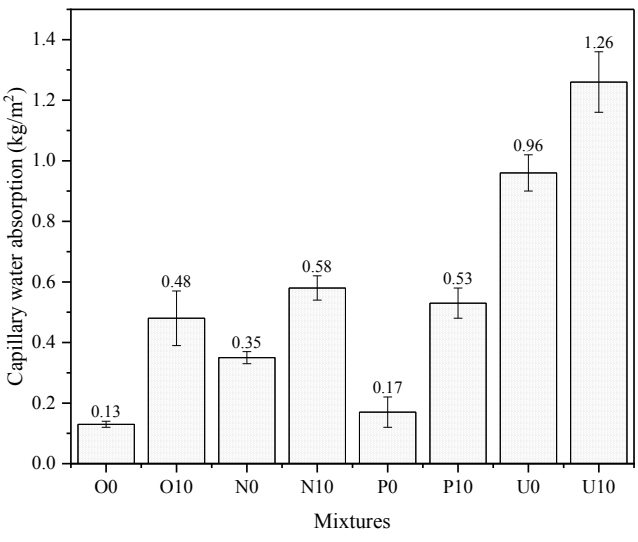

Fig. 9. Capillarity water absorption of concrete samples.

Fig. 10 shows the relationship of 28-day compressive strengths with capillary water absorption and hardened unit weights. The increase in the compressive strength of the concrete samples decreases the capillary water absorption values parabolic and increases the hardened unit weights parabolic. As the compressive strength of concrete mixes increases, the capillary void volume decreases. Therefore, the capillary water absorption of mixtures with high compressive strength decreases. As the unit weight of the mixtures increases, the compressive strength also increases. This is another indicator showing that the capillary void volume in the mixture has decreased.

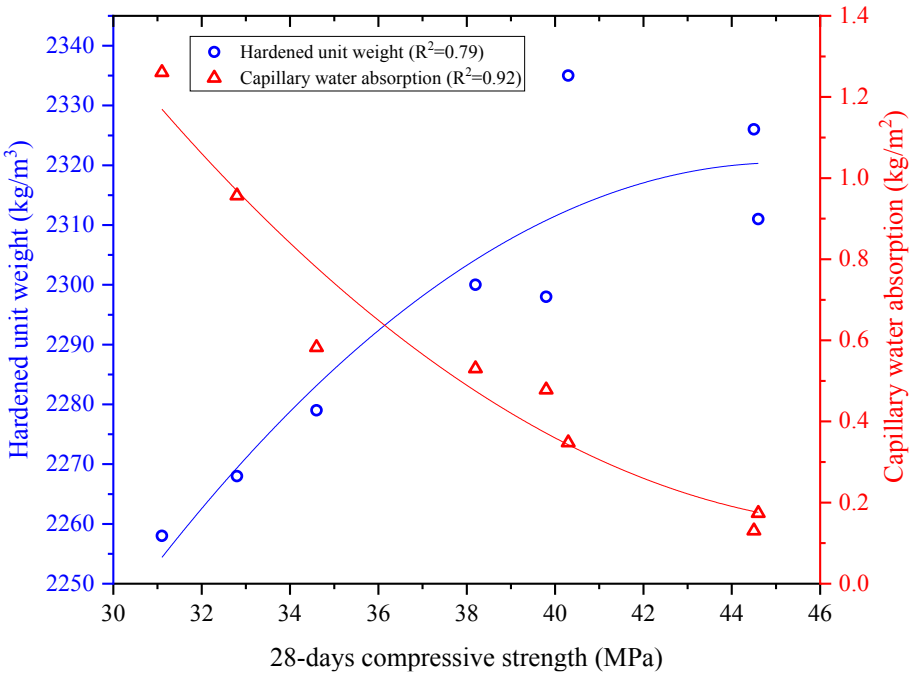

Fig. 10. The relationship of 28-day compressive strength of concrete samples with capillary water absorption and hardened unit weights.

3.4. Analysis of microstructural results

SEM images in Fig. 11 were obtained from the mortar phase of the mixtures. It was observed that SEM images obtained from different mixtures were similar to each other. As seen in the SEM images, it is seen that the matrix is dense. Due to the dense microstructure formed, the target compressive strength was achieved in the mixtures. A dense CSH gel was observed in the P10 mixture, with a compressive strength of about 40 MPa. In addition, it was observed that the interfacial transition (ITZ) region between the aggregate and the matrix was intense. Microcracks were observed in some regions of the matrix. These cracks were mostly formed after the compressive strength test. In addition, micro limestone particles smaller than 50 µm were also seen in the matrix. The microstructure condensation property of micro limestone particles was determined. As a result of the hydration reaction, needle-like CSH gels were formed. In addition, spherical air voids were determined in the matrix. These air voids were formed due to insufficient vibration. The air voids formed are usually less than 50 µm in diameter. In particular, SEM images show that micro limestone is more concentrated in some regions. This indicates that the micro limestone tends to agglomerate. As a result, a dense microstructure was observed in SEM images. It has also been determined that hydration products such as CSH are formed.

4. Conclusions

The usability of the concretes, which are obtained by natural means and formed with aggregates found in Erzurum region, on concrete pavements was investigated for the mechanical properties, physical properties, capillary water absorption, and microstructural structure of the micro limestone or non-limestone concrete mixes formed with these aggregates, in this work. The results of the study are summarized below.

- The use of micro limestone reduced the unit weights of the mixtures. However, since the specific weights of natural aggregates are close to each other, the unit weights are very close to each other.
- 7 and 28 days, the mixtures' mechanical properties (compressive and flexural strength) using micro limestone decreased. However, if micro limestone is used, C30/37 class concretes can also be produced. Similarly, micro-limestone reduced the 7- and 28-day flexural strengths of concretes. As the compressive strength of concrete mixtures increased, the flexural strength also increased. Maximum compressive and flexural strengths were obtained in the concretes formed with the aggregates taken from the Oltu and Pasinler regions.
- Since micro limestone increases the capillary void volume, the capillary water absorption of the mixtures increases. Especially the aggregates belonging to the Uz-

undere region increased the capillary water absorption considerably. On the other hand, aggregates in the Oltu region reduced capillary water absorption.

- Micro limestone particles with cement fineness were observed in SEM images. Micro limestone grains have concentrated the microstructure. In addition, needle-like CSH gels were formed due to hydration.
- As a result, it has been determined that concrete pavements can be produced with natural aggregates from the Erzurum region. Even when 10% micro limestone is used instead of cement, C30/37 class concretes can be produced. In this way, more environmentally friendly concrete pavements will be made.

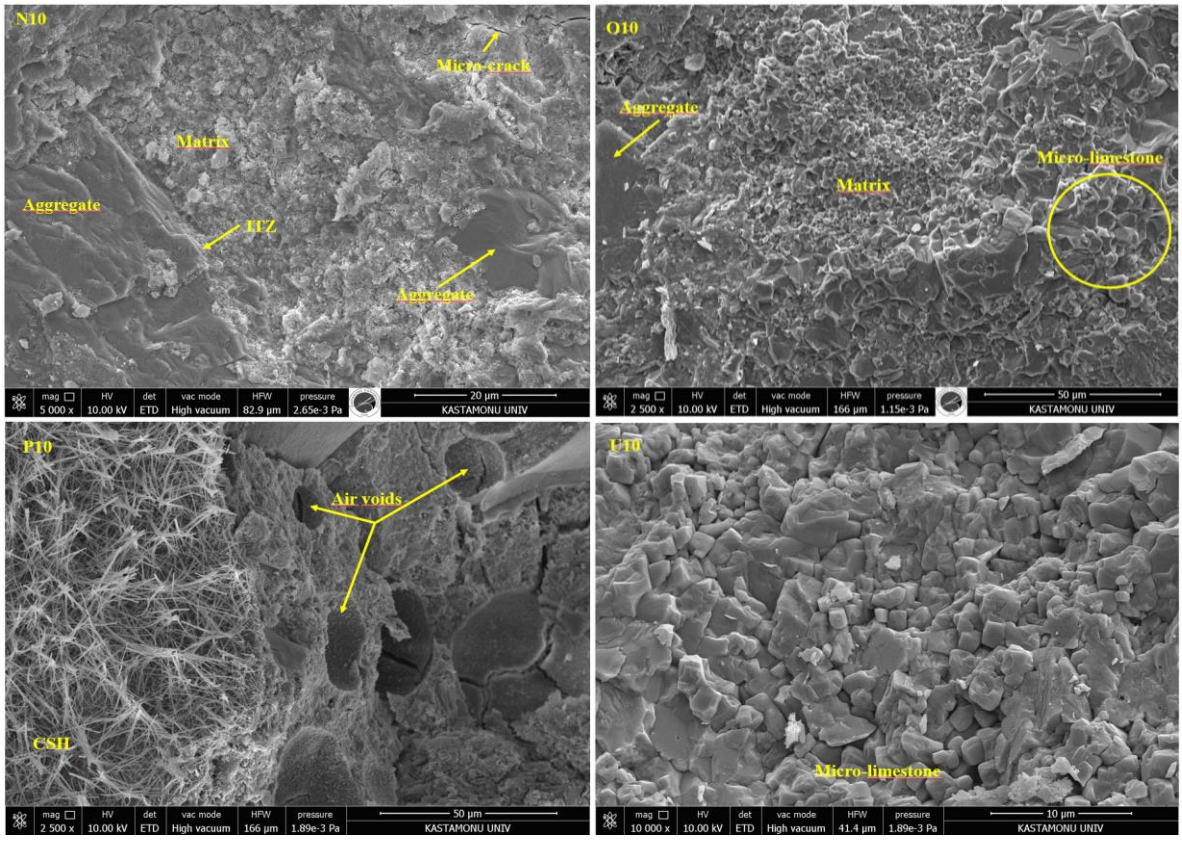

Fig. 11. SEM images of mixtures.

Acknowledgements

This study was carried out using wet concrete experiments, molding and curing processes in Atatürk University Narman Vocational School Construction Materials Laboratory. Hardened concrete experiments were performed in Atatürk University Civil Engineering Structural Mechanics and Construction Materials Investigation Laboratory.

Funding

This study was funded within the scope of ATATEKNOKENT R&D project (Project code: STB 066347).

Conflict of Interest

The author declared no potential conflicts of interest with respect to the research, authorship, and/or publication of this manuscript.

References

Acar MC (2022). Usability of Kayseri volcanic slags as filling material on flexible paved roads. *Journal of the Faculty of Engineering and Architecture of Gazi University*, 37(1), 47-56.

ACI 522R-10 (2010). Report on Pervious Concrete. ACI Comitee 522, American Concrete Institute, USA.

Airey GD (2002). Rheological evaluation of ethylene vinyl acetate polymer modified bitumens. *Construction and Building Materials*, 16(8), 473-487.

ASTM C33-16 (2016). Standard Specification for Concrete Aggregates. ASTM International, United States.

ASTM C348 (1998). Standard Test Method for Flexural Strength of Hydraulic-Cement Mortars. ASTM International, United States.

ASTM C349 (2002). Standard test method for compressive strength of hydraulic-cement mortars (Using portions of prisms broken in flexure). ASTM International, United States.

ASTM C642 (1997). Standard Test Method for Density, Absorption, and Voids in Hardened Concrete. ASTM International, United States.

ASTM C944 (2019). Standard Test Method for Abrasion Resistance of Concrete or Mortar Surfaces by the Rotating-Cutter Method. ASTM International, United States.

Bekem Kara İ (2020). Effect of the use of calcite as a substitute for cement on compressive strength. *Journal of Investigations on Engineering & Technology*, 3(1), 10-16.

Budak G, Ünlu M, Minta S (2009). Introduction of a laboratory mix design method for roller compacted concrete pavements in Turkey. *6th International Conference on Maintenance and Rehabilitation of Pavements and Technological Control, MAIREPAV 2009*.

Chandrappa AK, Biligiri KP (2016). Pervious concrete as a sustainable pavement material-Research findings and future prospects: A state-of-the-art review. *Construction and Building Materials*, 111, 262-274.

Delongui L, Matuella M, Núñez WP, Fedrigo W, Silva Filho LCP da, Ceratti JAP (2018). Construction and demolition waste parameters for rational pavement design. *Construction and Building Materials*, 168, 105–112.

Ebrahimi Besheli A, Samimi K, Moghadas Nejad F, Darvishan E (2021). Improving concrete pavement performance in relation to combined effects of freeze–thaw cycles and de-icing salt. *Construction and Building Materials*, 277, 122273.

Eisa MS, Fahmy EA, Basiouny ME (2022). Using metakaolin-based geopolymer concrete in concrete pavement slabs. *Innovative Infrastructure Solutions*, 7(1), 1-11.

EN 197-1 (2004). Composition, Specifications, and Conformity Criteria for Common Cements. European Standard.

EN 12350-2 (2009). Testing Fresh Concrete - Part 2: Slump test. European Standard.

EN 12390-2 (2009). Testing Hardened Concrete - Part 2: Making and Curing Specimens for Strength Tests. European Standard.

Harrington D, Abdo F, Adaska W, Hazaree C (2010). Guide for roller-compacted concrete pavements. *Institute for Transportation, Iowa State Univerisity*, August, 104.

Isacsson U, Lu X (1995). Testing and appraisal of polymer modified road bitumens-state of the art. *Materials and Structures*, 28(3), 139-159.

Keleş ÖF, Akpinar MV (2022). Strength properties of roller compacted concrete pavement (RCCP) under different curing methods. *Construction and Building Materials*, *324*, 126530.

Komastka SH, Kerkhoff B, Panarese WC (2003). Design and Control of Concrete Mixtures. Preface and Acknowledgments. Portland Cement Association, USA.

Kozak M (2011). Investigation of concrete roads and concrete road construction. *Electronic Journal of Construction Technologies*, 7(7), 89-99.

Lam MNT, Le DH, Jaritngam S (2018). Compressive strength and durability properties of roller-compacted concrete pavement containing electric arc furnace slag aggregate and fly ash. *Construction and Building Materials*, 191, 912–922.

Lee EB, Lee H, Akbarian M (2005). Accelerated pavement rehabilitation and reconstruction with Long-Life asphalt concrete on high-traffic Urban highways. *Transportation Research Record*, 56–64.

Nanni A, Ludwig D, Shoenberger J (1996). Roller compacted concrete for highway pavements. *Concrete International*, 18(5), 33-38.

Sangiorgi C, Lantieri C, Dondi G (2015). Construction and demolition waste recycling: An application for road construction. *International Journal of Pavement Engineering*, 16(6), 530-537.

Şengün E, Öztürk Hİ, Yaman İÖ (2020). Mekanistik-ampirik ve geleneksel beton yol tasarım yöntemlerinin karşılaştırılması: Afyon-Emirdağ deneme kesimi. *Teknik Dergi*, 31(5), 10251–10274. (in Turkish)

Strieder HL, Dutra VFP, Graeff ÂG, Núñez WP, Merten FRM (2022). Performance evaluation of pervious concrete pavements with recycled concrete aggregate. *Construction and Building Materials*, 315, 125384.

Suo Z, Wong WG (2009). Nonlinear properties analysis on rutting behaviour of bituminous materials with different air void contents. *Construction and Building Materials*, 23(12), 3492–3498.

Challenge Journal of Concrete Research Letters

Research Article

Minimum weight design of reinforced concrete beams utilizing grey wolf and backtracking search optimization algorithms

Osman Tunca [a,*], Serdar Çarbaş [a]

[a] *Department of Civil Engineering, Karamanoğlu Mehmetbey University, 70200 Karaman, Turkey*

ABSTRACT

In this study, optimal weight design of a reinforced concrete beam subjected to various loading conditions is investigated. The purpose of the optimization is to attain the minimum weight design of the reinforced concrete beam under distributed and two-point loads. The design problem is handled under three different design load cases. The two-point loads are affected on beam-to-beam connection nodes of reinforced concrete beams. Thus, while the magnitudes of distributed load and two-points load are remained constant, the distances between two-points loads are taken as 2m, 3m and 4m, respectively. The width and height of the rectangular cross-section of the concrete beam, and the diameters of the longitudinal and confinement steel rebars are treated as design variables of the optimum design problem. The design constraints of the optimization problem consist of the geometric constraints and necessities of the Turkish Requirements for Design and Construction of Reinforced Concrete Structures (TS500), and Turkish Building Earthquake Code (TBEC). As two novel metaheuristics, grey wolf (GW) and backtracking search (BS) optimization algorithms are selected as optimizers. Both algorithms are independently operated five times for three different design problems. Thus, the obtained results are examined statistically to compare in accordance with algorithmic performances. The optimal findings from optimization algorithms show that the GW algorithm is a little bit more robust on the exploitation phase, while the BS algorithm is stronger on the exploration phase. Moreover, it can be deducted from optimal beam designs that the GW algorithm is more viable to minimize reinforced concrete beam design.

ARTICLE INFO

Article history:
Received 6 May 2022
Revised 27 May 2022
Accepted 2 June 2022

Keywords:
Reinforced concrete beams
Metaheuristics
Minimum weighted design
Grey wolf optimizer
Backtracking search optimization

1. Introduction

The engineering design is generally based on the requirements of safety, economy and aesthetics, respectively. In this context, it is not enough for the design to fulfill the safety requirements alone. However, when all these requirements are considered, a hard to solve engineering design problem is confronted. Moreover, in some engineering design problems, some preliminary assumptions must be made in order to operate the required mathematical computations. For example, in order to design a steel structural member, first of all, the design loads acting on this member must be known. Hence, the internal forces of the element are calculated, and then the profile to be assigned to the structural element is selected according to these calculated loads. Yet, the design loads on the structural element are directly related to the dead load and the section to be selected (Tunca 2022). In the design of a reinforced concrete beam, to calculate the area of longitudinal steel rebars, first of all, the cross-sectional dimensions of the reinforced concrete beam should be instinctively selected. In some cases, the selected section sizes are insufficient and/or excessive (Coello et al. 1997; Hasan et al. 2019). Practically, the required dimensions are tried to be found by trial-and-error method. So, new calculation methods are needed to obtain the optimal design (Abubakar et al. 2021). At this point, the stochastic optimiza-

* *Corresponding author*. Tel.: +90-338-226-2200 ; Fax: +90-338-226-2214 ; E-mail address: osmantunca@kmu.edu.tr (O. Tunca)
ISSN: 2548-0928 / DOI: https://doi.org/10.20528/cjcrl.2022.02.003

tion methods come into the picture. These methods, tackle with objective or objectives, design variables, and design constraints of handled engineering design problem (Aydogdu 2016). In structural engineering, the objectives can be categorized as minimizing the cost of a structure while maximizing the structural responses under external loads (Jin et al. 2021). The design variables can be related to material property and geometry of the structure (Carbas et al. 2021). Some constraints are needed to ensure that the structures or structural elements are serviceable and comply with the relevant practical structural provisions. These are often selected as displacement, drift, or strength (Aydogdu 2016).

In this study, it is aimed to minimize weight of a single span reinforced concrete beam which is subjected to three different load cases. The height and width of the reinforced concrete beam, and the diameters of the longitudinal and confinement steel rebars are considered as design variables. Additionally, the optimum designs are intended to comply with Turkish Requirements for Design and Construction of Reinforced Concrete Structures (TS500 2000), and Turkish Building Earthquake Code (TBEC 2018). The constraints of the design optimization problem consist of the geometric constraints and necessaries of these requirements.

There are various optimization techniques applied to accomplish optimum designs of reinforced concrete structures and/or elements (Lu et al. 2021; Fahr et al. 2022). In this study, metaheuristic optimization methods are utilized as optimizer that do not require any derivative operations and initial gradient information (Kazemzadeh Azad and Aminbakhsh 2022). These methos offer designers convenience and ease in solving complex engineering design problems (Peng et al. 2022). Moreover, the stochastic based metaheuristic methods are also suitable for design problems involving nonlinear material and/or geometry. However, the solution of these problems is time consuming and it cannot be claimed that the obtained results are global optimum. In these kinds of problems, the design variables must be calculated as discrete ones (Erdal et al. 2016). In instance, the standard diameters of steel rebars are practically taken as 8mm, 10mm, or 12mm. Thus, to produce an optimally designed reinforced concrete beam, the selection of the steel rebars must be made amongst these values.

From past to now, numerous stochastic based metaheuristic optimization methods have been developed. Genetic algorithm (Goldberg and Holland 1988), harmony search method (Geem et al. 2016), particle swarm optimization (Perez and Behdinan 2007), firefly algorithm (Yang 2010) are some examples of so-called classical ones. To overcome their shortcuts and to enhance their algorithmic performances in finding the optimum results, so many brand-new stochastic optimization algorithms have been emerged day by day. The polar optimization algorithm (Chen et al. 2022), human felicity algorithm (Verij kazemi and Fazeli Veysari 2022), trees social relations optimization algorithm (Alimoradi et al. 2022) are the latest examples of novel metaheuristic optimization techniques. In this study, the grey wolf (GW) (Mirjalili et al. 2014) and backtracking search (BS) (Civicioglu 2013) optimization algorithms that are verified as successful to reach optimum results in the many engineering design problems, are executed. Both algorithms are tested on reinforced concrete beam design problems subjected to various loading conditions. Thus, both the optimum designs of reinforced concrete beams are obtained and the performances of two innovative optimization algorithms in obtaining optimum results are compared over the considered design problems.

The sections of the manuscript can be summarized as follows;

- In the Introduction section, the general concept of the study is defined.
- The practical design rules of the reinforced concrete beams are given in the second section.
- In the third section, the utilized stochastic based metaheuristic optimization methods are described.
- The design examples and obtained solutions and results are exhibited in the fourth section.
- The principal conclusions are presented in the fifth section.

2. Design Rules of Reinforced Concrete Beams

The design of a reinforced concrete beam having minimum design weight is considered as the objective of the optimization problem. The general illustration of the reinforced concrete beam design problem is given in Fig. 1. In Eq. (1), the $\boldsymbol{I^T}$ vector consists of sequence numbers of the height and width of the reinforced concrete beam, and diameters of the longitudinal and confinement steel rebars. Thus, it includes four different design variables.

$$\boldsymbol{I^T} = [I_1, I_2, I_3, I_4] \tag{1}$$

The weight of the reinforced concrete beam can be determined multiplying the volume and the unit weights of the components as shown in Eq. (2).

$$W = \rho_c\, h\, b_w L_b + \rho_s \left(n \frac{\pi \emptyset^2}{4} L_l + n_c \frac{\pi \emptyset_e^2}{4} L_c \right) \tag{2}$$

Here, ρ_c and ρ_s are the unit weights of the concrete and steel. The h and b_w are the height and width of the reinforced concrete beam. L_b, L_l and L_c represent the lengths of the beam, longitudinal and confinement steel rebars, respectively. $\emptyset$ and $\emptyset_e$ are diameters of the longitudinal and confinement steel rebars, and n and n_c are total number of these.

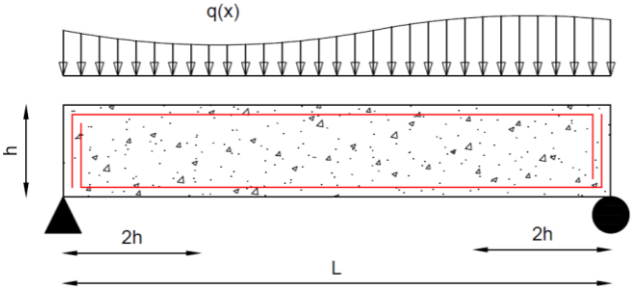

Fig. 1. The reinforced concrete beam.

In the first part of design problem, the height and width of the reinforced concrete beam should be determined. Here, if these are chosen small, the cross-section of the concrete part of the beam may be insufficient. If these are chosen large, it will be an uneconomical engineering design. The calculation of reinforced concrete beams is based on the assumption that the concrete part of the beam bear only compression loads. Therefore, the location of the neutral axis must be found. The distribution of compression loads in the cross-section is not uniform as seen Fig. 2a. However, for ease of calculation, the length of the neutral axis (c distance), is converted to uniform by multiplying the k_1 factor (Fig. 2b).

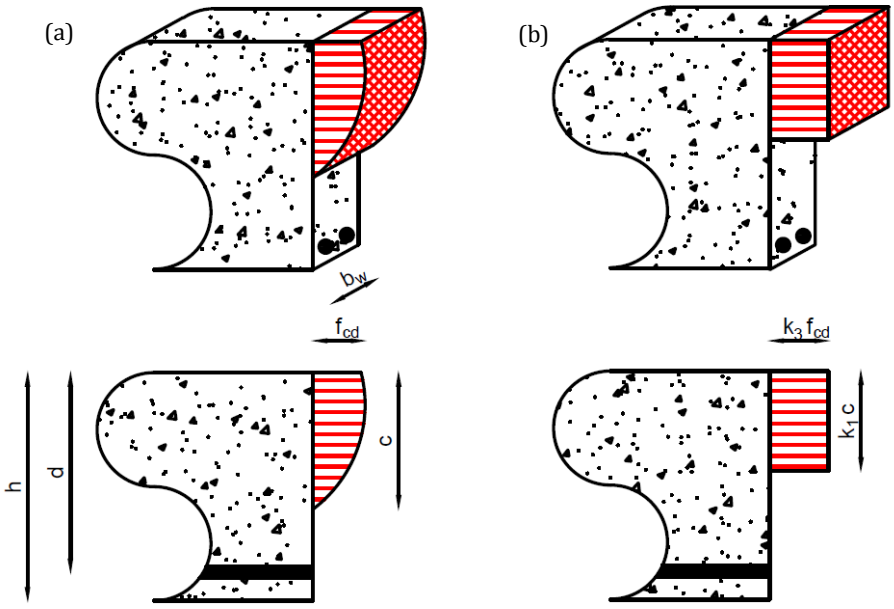

Fig. 2. Compressive stress distribution on the cross-section of the reinforced concrete beam: (a) Real distribution; (b) Uniform distribution.

The height of the effective compression area can be calculated using Eq. (3).

$$k_1 c = d - \sqrt{d^2 - \frac{2M_d}{k_3 f_{cd} b_w}} \tag{3}$$

Here, $k_1 c$ is location of reduced neutral axis, d is effective height, M_d is the design moment, and $k_3 f_{cd}$ is reduced concrete design strength. In such a reinforced concrete beam, the compressive force carried by the concrete and the total tensile force carried by the steel rebars should be equal. So, the total area of the longitudinal reinforcement (A_s) is generated easily via Eq. (4).

$$A_s = \frac{M_d}{f_{yd}\left(d - \frac{k_1 c}{2}\right)} \tag{4}$$

The number of longitudinal steel rebars (n) is determined through Eq. (5). In the mentioned equation, the *int* represents the integer transformation function. Here, the diameter of the longitudinal reinforcement is predetermined by designer.

$$n = int\left(\frac{A_s}{\frac{\pi \emptyset}{4}}\right) + 1 \tag{5}$$

The length of the longitudinal steel rebars is required to determine the quantities. This is determined according to Fig. 1.

The confinement steel rebars reinforce the beam to the shear loads. These are handled in two regions as confinement zone and remaining zone. The shear force at a distance d from the column face is considered for confinement zone. In the other, this distance is taken as $2h$. Before the calculation of confinement steel rebars, the cross section of the reinforced concrete beam is checked utilizing Eq. (6).

$$V_{d-\max} = 0.85\, b_w h \sqrt{f_{ck}} \tag{6}$$

Here, V_{d-max} is the maximum designable shear carrying capacity of the reinforced concrete beam. The characteristic pressure strength of the concrete is represented as f_{ck}. The critic shear force is calculated considering the unreinforced condition of the concrete beam using Eq. (7).

$$V_{cr} = 0.65\, f_{ctd}\, b_w d \tag{7}$$

Here, V_{cr} is critic shear force and f_{ctd} is the tension design strength of the concrete. The shear force carried by the steel rebars is calculated via Eq. (8).

$$V_w = V_d - 0.8\, V_{cr} \tag{8}$$

The minimum amount of steel rebar determined by structural specifications can be calculated from Eq. (9). Here, the double-armed confinement steel rebar is utilized for beam modelling since this kind of confinement

steel rebars are practically implemented in real-life reinforced concrete beam applications too often.

$$S_c = min\begin{pmatrix} \frac{A_{sw} f_{ywd} d}{V_w} \\ \frac{h}{4} \\ 8Ø \\ 150mm \end{pmatrix} \quad (9)$$

Here, S_c is the distances between two confinement steel rebars. In the remaining zone, this value is symbolized with S_o, and determined via Eq. (10).

$$S_o = min\begin{pmatrix} \frac{A_{sw} f_{ywd} d}{V_w} \\ if\ V_d \le 3V_{cr}\ then\ S_o = \frac{d}{2} \\ if\ V_d > 3V_{cr}\ then\ S_o = \frac{d}{4} \end{pmatrix} \quad (10)$$

The obtained S_c and S_o are used to determine the total number of the confinement steel rebars (n_c).

$$n_c = int\left(\frac{4d}{S_c} + 1\right) + int\left(\frac{L-4d}{S_c} + 1\right) \quad (11)$$

The lengths of the confinement steel rebars are calculated considering Fig. 3. As the hook length of the confinement steel rebars, the biggest one of 6Øe and 8 cm is accepted as the minimum value.

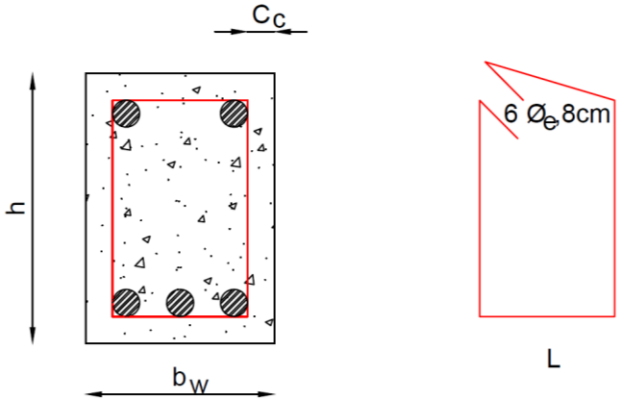

Fig. 3. Confinement rebars of reinforced concrete beam.

Finally, it should be checked that the determined steel rebars fits into the cross section of the reinforced concrete beam as illustrated in Fig. 4. For this aim, Eq. (12) is utilized.

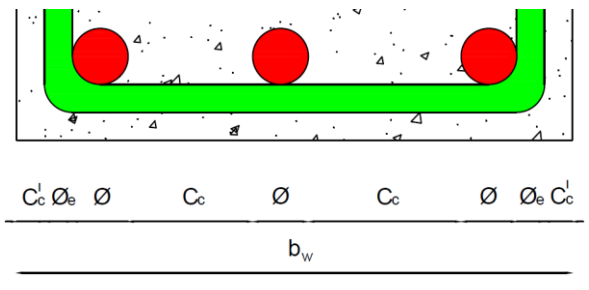

Fig. 4. Settlement of reinforcements.

$$b_w \ge 2C_c' + 2Ø_e + nØ + (n-1)C_c \quad (12)$$

Here, C_c' is the thickness of concrete cover, and C_c is the distance between longitudinal steel rebars.

3. Optimization Methods

In this study, two recent metaheuristics, namely grey wolf (GW) and backtracking search (BS) optimization algorithm are utilized as optimizers to minimize the design weight of the reinforced concrete beam.

3.1. Backtracking search (BS) algorithm

Backtracking search (BS) algorithm is encoded by Civicioglu in 2013. BS has only a single control parameter, and simple and effective algorithmic structure. It consists of five main steps such as initialization, selection-I, mutation, crossover, and selection-II. In the first step, the population size, the total number of dimensions, the lower and upper bounds of the design variables are defined. Then, initial population is obtained utilizing Eq. (13).

$$P_{i,j} \sim U(low_j, up_j) \quad (13)$$

Here, U symbolizes uniform distribution probability and, $P_{i,j}$ is possible solution value.

The historical population is generated in the selection-I step. When initial P_{old} is generated, this based on randomization as in P. Then, Eq. (14) is utilized for the other iterations.

$$\text{if } a < b \text{ then old}P := P|a, b \sim U(0,1)| \quad (14)$$

In Eq. (14), a and b are generated randomly between 0 and 1. If b is bigger than a, the element of the P_{old} is shifted with the element of P. Otherwise, the element value of P_{old} is saved as memory of BS. Then, the order of the elements in P_{old} is permuted using Eq. (15).

$$\text{old}P := Permuting(\text{old}P) \quad (15)$$

In the mutation step, the form of the trial population $Mutant$ is obtained via Eq. (16).

$$Mutant = P + F\ (\text{old}P - P) \quad (16)$$

Here, F represents an adjusting coefficient of the search direction amplitude that is randomly generated in each iteration. The trial population is shaped final form in crossover step. The crossover step has two main stages. Initially, the binary integer-valued matrix (map) is created based on randomization. The map consists of the 0 and 1 values. Here, the dimensions of the T, P, and map are same. On condition that, element of the map is 0, element of T is saved. Otherwise, the element of the T is manipulated with the element of the P in same matrix index. In case the values exceed the upper and lower boundaries, the limit values are assigned instead of these values.

Finally, the global minimum value is checked in selection-II step. If the old *global minimum value* that is better than the fitness of best vectors of P (P_{best}), it is saved. Otherwise, The P_{best} is saved as the *global minimum value*.

3.2. Grey wolf (GW) algorithm

Grey wolf (GW) algorithm was encoded by Mirjalili et al. (2014). It imitates the social and hunting behaviors of grey wolves (Canis lupus). The grey wolfs have hierarchical characteristics. They move together to hunt preys. There are three dominant grey wolf named alpha (α), beta (β), and omega (ω). The domination is getting increase from ω to α.

In a hunting, the grey wolves group encircles the prey at the beginning. This behavior of grey wolves is operated via Eqs. (17) and (18).

$$\vec{D} = \left|\vec{C}\vec{X}_p(t) - \vec{X}(t)\right| \tag{17}$$

$$\vec{X}(t+1) = \vec{X}_p(t) - \vec{A}\vec{D} \tag{18}$$

Here, the number of iterations is symbolized with t. The $\vec{X}$ and $\vec{X}_p$ represent the locations of grey wolves and prey, respectively. The expression of $\vec{A}$ and $\vec{C}$, which are the coefficient vectors, are given in Eqs. (19) and (20).

$$\vec{A} = 2\,\vec{a}\vec{r}_1 - \vec{a} \tag{19}$$

$$\vec{C} = 2\,\vec{r}_2 \tag{20}$$

Here, $\vec{r}_1$ and $\vec{r}_2$ are randomly generated between 0 and 1. In the iterative process, $\vec{a}$ is linearly reduced 2 to 0.

The hunting starts after the encircling process. The most dominant gray wolf α manages the hunt. However, sometimes β and ω also contribute to management. So, the positions of the grey wolves are relocated consistent with the results of α, β, and ω. Eqs. (21) to (23) are performed for this purpose.

$$\vec{D}_\alpha = \vec{C}_1\vec{X}_\alpha - \vec{X}, \quad \vec{D}_\beta = \vec{C}_2\vec{X}_\beta - \vec{X}, \quad \vec{D}_\delta = \vec{C}_3\vec{X}_\delta - \vec{X} \tag{21}$$

$$\vec{X}_1 = \vec{X}_\alpha - \vec{A}_1(\vec{D}_\alpha), \qquad \vec{X}_2 = \vec{X}_\beta - \vec{A}_2(\vec{D}_\beta),$$
$$\vec{X}_3 = \vec{X}_\delta - \vec{A}_3(\vec{D}_\delta) \tag{22}$$

$$\vec{X}(t+1) = \frac{\vec{X}_1+\vec{X}_2+\vec{X}_3}{3} \tag{23}$$

The hunting step of the algorithm is completed by terminating the repositioning. Here, the $\vec{A}$ starts to decrease due to the decrease in $\vec{a}$. The reduction of the value of $\vec{A}$ impress the gray wolves to hunt.

4. Design Examples

Three reinforced concrete beams having three different mid-spans (a distance) are considered as design examples as showed in Fig. 5. All of them has 6m of total span length. They are placed on columns having 400 mm wide at its supports. The yield strength of the concrete and steel rebars are taken as 25 MPa and 420 MPa, respectively. The safety factors are considered as 1.5 for concrete and 1.15 for steel. The unit weights of them are taken as 24 kN/m^3 and 76.98 kN/m^3, respectively. The distributed loads of 25kN/m and two-point loads of 100kN are assigned as design loads as shown in Fig. 5. Here, the two-point loads represent the beam connection joints, and the distance between them varies from structure to structure. So, the distance between two-points loads (a distance) is taken as 2m, 3m, and 4m for reinforced concrete beams.

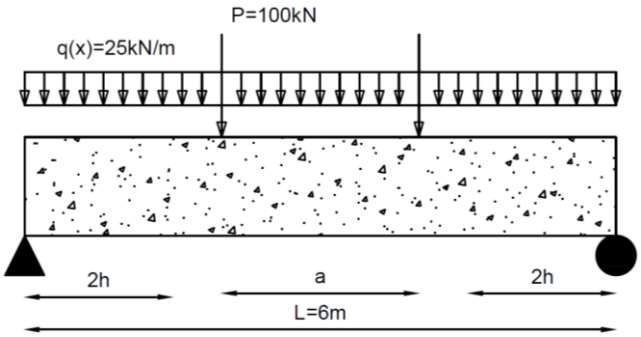

Fig. 5. General scheme of reinforced concrete beam.

The minimum design weight is considered as objective. Before solving such a concrete beam design problem, the b_w and h values should be estimated. So, these are taken as first two design variables. After their estimation, the required amount of steel rebars can easily be calculated. However, the selection of the diameters of rebars is also needed to complete the design. Thus, the diameter of longitudinal steel rebars and confinement steel rebars are also treated as design variables. To obtain viable design, the structural necessities for design constraints are taken from Turkish Requirements for Design and Construction of Reinforced Concrete Structures (TS500 2000), and Turkish Building Earthquake Code (TBEC 2018). As addition to these, the geometric constraint is considered as the steel rebars fits into the cross section of the reinforced concrete beam. The population size is taken as 20 for both algorithms. The adjusting coefficient (F) of the BS algorithm is considered as 3 and the (α) parameter of the GW algorithm is linearly reduced from 2 to 0. The number of iterations is taken as 500 in each optimization process. So, the total number of required structural analyses is taken as 500×20=10000.

The optimum designs of the reinforced concrete beams are independently obtained via GW and BS algorithms as given in Table 1. From this table, it is clearly seen that there are no any violations on design constraints in optimally designed beams. Besides, the most dominant design constraint is the geometric constraint which checks whether steel rebars fits into the cross section of the reinforced concrete beam or not. Moreover, in order to statistically evaluate the attained optimal design solutions, each algorithm is executed on the same design example for five times. Among these, the minimum design weight histories of the algorithms are illustrated in Fig. 6. In the first design example, which has 2 m distances between two-points

loads (a=2m in Fig. 5), the GW and BS algorithms attain the same optimal design weight of 17.317 kN. However, the GW and BS algorithms require 377 and 221 structural analyses to reach minimum design weights, respectively. It means that in the first design example, the BS algorithm require 70.59% structural analyses than the GW algorithm. In the second design example, which has 3m distances between two-points loads, the GW algorithm does not only find a lighter beam design, but also converge 21.37% faster than BS algorithm since it needs only 234 structural analyses. In the third and final design example, which has 4 m distances between two-point loads, both metaheuristic optimization algorithms show almost identical algorithmic performances. They generate same minimum optimal design weight of 14.534 kN. But to accomplish this design weight the GW algorithms show 10% faster convergence rate than BS algorithm.

Furthermore, the accomplished statistical results are tabulated in the Table 1. Here, the worst weight, the average weight, and the standard deviation values are presented to illustrate the dispersion between optimal design weights attained from five different initial populations via GW and BS optimization algorithms. The relatively lower standard deviations indicates that the obtained minimum design weights are tend to be smoothly scattered around the average weights and the box-plots of these executions are illustrated in Fig. 7. From these findings, it can be deduced that although the BS algorithm seems as more successful in the design of reinforced concrete beams with a distance of 2 m between two-points loads, the statistical data indicates that the GW algorithm puts forward more stable and more consistent performance in attaining the final optimum design of reinforced concrete beams.

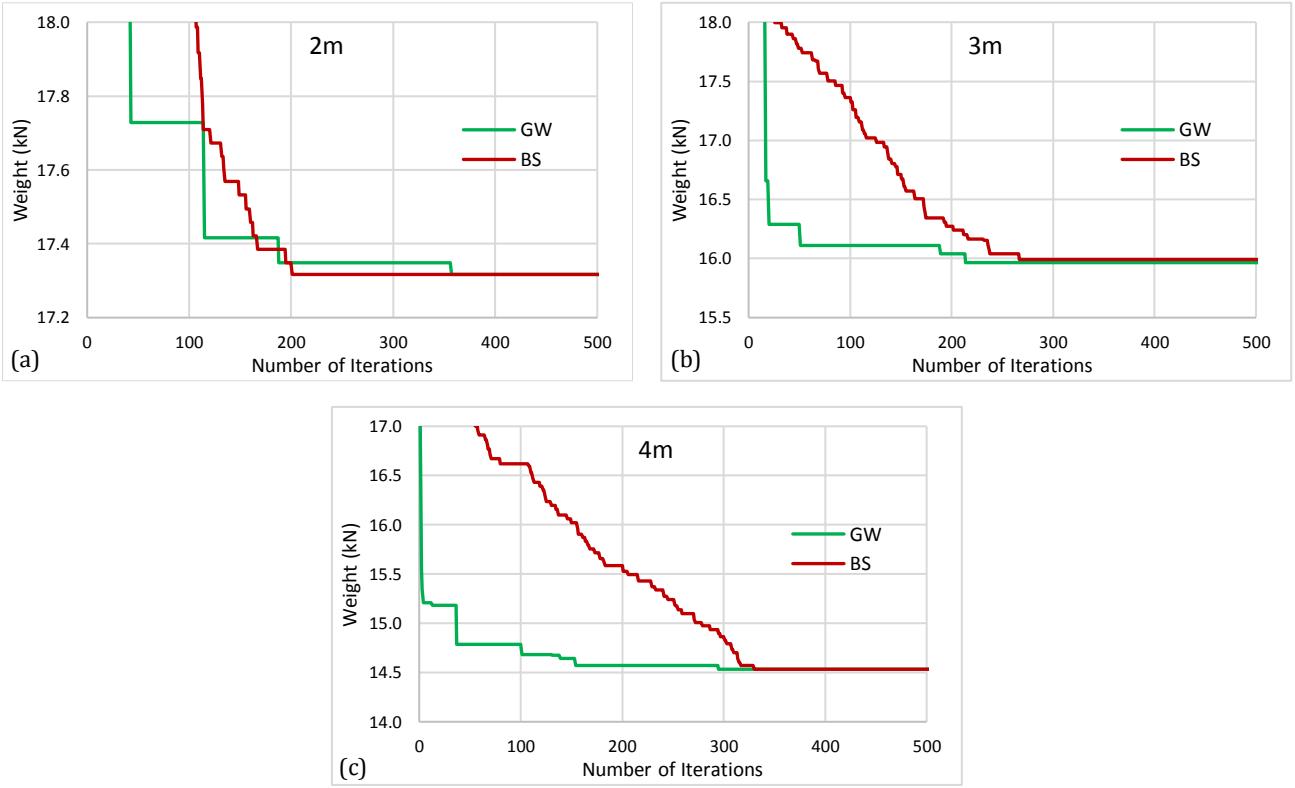

Fig. 6. Design histories of reinforced concrete beams having a) 2m; b) 3m; and c) 4m between two-point loads.

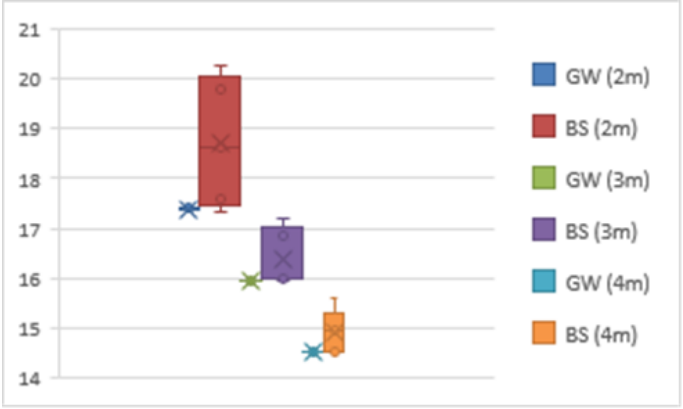

Fig. 7. Box-plots of obtained optimum reinforced concrete beams.

Table 1. Optimum design results of reinforced concrete beams.

Distance between two-point loads	2 m		3 m		4 m	
Algorithm	BS	GW	BS	GW	BS	GW
b_w (mm)	252	252	251	250	250	250
h (mm)	468	468	433	434	394	394
$Ø_e$	8	8	8	8	8	8
Ø	40	40	38	38	38	38
$g(1)$	-0.439	-0.439	-0.430	-0.431	-0.490	-0.490
$g(2)$	-0.872	-0.872	-0.872	-0.872	-0.872	-0.872
$g(3)$	0.000	0.000	-0.020	-0.016	-0.016	-0.016
Weight (kN)	17.317	17.317	15.992	15.966	14.534	14.534
No. of required structural analyses	221	377	287	234	350	315
Worst weight (kN)	20.265	17.394	17.189	15.966	15.596	14.534
Standard deviation	1.307	0.035	0.578	0.000	0.435	0.000
Average weight (kN)	18.718	17.379	16.395	15.966	14.916	14.534

5. Conclusions

The optimum design of reinforced concrete beams having three different mid-span lengths between two-point loads as 2 m, 3 m, and 4 m are obtained. Finding the minimum design weights of the beams are taken as main objective. When the design weights of the reinforced concrete beams are calculated, the confinement steel rebars are considered as well as the weight of the concrete and longitudinal steel rebars. The design variables are set as discrete values in order to make possible of fabrication the designed beams. To do this, the structural necessities from Turkish Requirements for Design and Construction of Reinforced Concrete Structures (TS500 2000), and Turkish Building Earthquake Code (TBEC 2018) are considered. So, totally three optimum design problems are handled utilizing the grey wolf (GW) and backtracking search (BS) optimization algorithms for this purpose. Thus, both the optimum designs of reinforced concrete beams are found and the performances of metaheuristic optimization algorithms are compared. Both algorithms are independently operated five different times for each design example. By this means, the obtained results are statistically examined and discussed. The principal conclusions of this study can be itemized as in the following bullet points:

- The GW and BS algorithms can robustly be used as the design optimizer to minimum weight design of reinforced concrete beams.
- The GW and BS algorithms accomplish identical minimum design weight of 17.317 kN for design example having 2 m distance between two-point design loads. However, to produce this optimum design weight the BS and GW algorithms require 221 and 377 structural analyses, respectively. So, BS algorithm computationally performs 70.59% better than GW algorithm for the first design example. Yet, in other design examples, the algorithmic performance of the GW algorithm is better than BS algorithm.
- The design history graphs prove that while BS algorithm has better exploration capacity, the GW algorithm has powerful in exploitation capacity.
- Finally, the statistical analyses illustrate the supremacy of GW algorithm in finding the minimum design weights of the reinforced concrete beams.

Acknowledgements

None declared.

Funding

The authors received no financial support for the research, authorship, and/or publication of this manuscript.

Conflict of Interest

The authors declared no potential conflicts of interest with respect to the research, authorship, and/or publication of this manuscript.

References

Abubakar J, Anum B, Iaren CT (2021). Design optimization of rectangular beams using genetic algorithm. *Journal of Engineering Sciences,* 4(2), 66–78.

Alimoradi M, Azgomi H, Asghari A (2022). Trees social relations optimization algorithm: A new Swarm-Based metaheuristic technique to solve continuous and discrete optimization problems. *Mathematics and Computers in Simulation*: 629–664.

Aydogdu I (2016). Cost optimization of reinforced concrete cantilever retaining walls under seismic loading using a biogeography-based optimization algorithm with Levy flights. *Engineering Optimization,* 49(3), 381–400,

Aydogdu I (2016). New Iterative method to Calculate Base Stress of Footings under Biaxial Bending. *International Journal of Engineering and Applied Sciences,* 8(4), 40–48.

Carbas S, Toktas A, Ustun D (eds) (2021). Nature-Inspired Metaheuristic Algorithms for Engineering Optimization Applications. Springer Tracts in Nature-Inspired Computing. Springer Singapore, Singapore.

Chen D, Ge Y, Wan Y, Deng Y, Chen Y, Zou F (2022). Poplar optimization algorithm: A new meta-heuristic optimization technique for numerical optimization and image segmentation. *Expert Systems with Applications*, 117118.

Civicioglu P (2013). Backtracking search optimization algorithm for numerical optimization problems. *Applied Mathematics and Computation,* 219(15), 8121–8144.

Coello CC, Hernández FS, Farrera FA (1997). Optimal design of reinforced concrete beams using genetic algorithms. *Expert Systems with Applications,* 12(1), 101–108.

Erdal F, Tas S, Tunca O, Carbas S (2016). Effect of random number sequences on the optimum design of castellated beams with improved harmony search method. *International Journal of Engineering and Applied Sciences,* 8(3), 25–39.

Fahr S, Mitsos A, Bongartz D (2022). Simultaneous deterministic global flowsheet optimization and heat integration: Comparison of formulations. *Computers & Chemical Engineering*, 107790.

Geem ZW, Kim JH, Loganathan GV (2016). A new heuristic optimization algorithm: Harmony search. *Simulation*, 76(2), 60–68.

Goldberg DE, Holland JH (1988). Genetic algorithms and machine learning. *Machine Learning,* 3(2): 95–99.

Hasan QF, Al-Mamany DA, Fayadh OK (2019) Design of reinforced concrete deep beams using particle swarm optimization technique. *Karbala International Journal of Modern Science,* 5(4), 255–265.

Jin C, Chung WC, Kwon DS, Kim MH (2021). Optimization of tuned mass damper for seismic control of submerged floating tunnel. *Engineering Structures*, 112460.

Kazemzadeh Azad S, Aminbakhsh S (2022). ε-constraint guided stochastic search with successive seeding for multi-objective optimization of large-scale steel double-layer grids. *Journal of Building Engineering*, 103767.

Lu S, Wang C, Fan Y, Lin B (2021). Robustness of building energy optimization with uncertainties using deterministic and stochastic methods: Analysis of two forms. *Building and Environment*, 108185.

Mirjalili S, Mirjalili SM, Lewis A (2014). Grey wolf optimizer. *Advances in Engineering Software*, 69, 46–61.

Peng H, Xiao W, Han Y, Jiang A, Xu Z, Li M, Wu Z (2022). Multi-strategy firefly algorithm with selective ensemble for complex engineering optimization problems. *Applied Soft Computing*, 108634.

Perez RE, Behdinan K (2007). Particle swarm approach for structural design optimization. *Computers & Structures,* 85(19–20), 1579–1588.

TBEC (2018). Turkish Building Earthquake Code Specifications for Design of Buildings under Seismic Effects, Ankara, Turkey.

TS500 (2000). Requirements for Design and Construction of Reinforced Concrete Structures, Standard TS500, Ankara, Turkey.

Tunca O (2022). Optimum design of a vaulted roof steel structure using grey wolf and backtracking search optimization algorithms through application programming interface. *Challenge Journal of Structural Mechanics*, 8(1), 1–8.

Verij kazemi M, Fazeli Veysari E (2022). A new optimization algorithm inspired by the quest for the evolution of human society: Human felicity algorithm. *Expert Systems with Applications*, 116468.

Yang XS (2010). Firefly algorithm, Lévy flights and global optimization. *Research and Development in Intelligent Systems XXVI: Incorporating Applications and Innovations in Intelligent Systems,* 17, 209–218.